

# High Brightness and Enhanced Stability of CsPbBr<sub>3</sub>-Based Perovskite Light-Emitting Diodes by Morphology and Interface Engineering

Xue Liu, Xiaoyang Guo,\* Ying Lv, Yongsheng Hu, Yi Fan, Jie Lin, Xiaomin Liu, and Xingyuan Liu\*

A CsPbBr<sub>3</sub>-based all-inorganic perovskite light-emitting diode (PeLED) with ultrahigh brightness and enhanced stability is prepared by controlling of morphology and interface engineering. A nonionic surfactant polyoxyethylene (20) sorbitan monolaurate is introduced into the CsPbBr<sub>3</sub> film, which induces tightly arranged grains in the perovskite film, thus highly passivating the defects at the grain boundaries, resulting in a performance-enhanced PeLED with a highest brightness of 111 000 cd m<sup>-2</sup>, a peak current efficiency (CE) of 21.1 cd A<sup>-1</sup>, a maximum external quantum efficiency (EQE) of 5.55%, and an operational lifetime of 4.5 h. The device properties are further improved by adding an anionic surfactant sodium dodecyl benzene sulfonate to modify the hole injection layer poly(ethylenedioxythiophene):polystyrenesulfonate. The hole current density is increased, further balancing the charge injection and transport. Finally, the optimal device displays an ultrahigh brightness of 179 000 cd m<sup>-2</sup>, a peak CE of 28.0 cd A<sup>-1</sup>, a maximum EQE of 7.39%, and a further prolonged lifetime of 6 h.

electroluminescent (EL) performance of CH<sub>3</sub>NH<sub>3</sub>PbBr<sub>3</sub> (MAPbBr<sub>3</sub>)-based green PeLED has been greatly boosted from a maximum current efficiency (CE) of 0.3–42.9 cd A<sup>-1</sup>.<sup>[6–8]</sup> And the record of the external quantum efficiency (EQE) is 14.36%, which is achieved by a quasi-two-dimensional green PeLED.<sup>[18]</sup> However, despite the rapid improvement of EL performance, the poor moisture and thermal stability of methylamine halide perovskites causes serious deterioration of PeLEDs, limiting their long-term applications.<sup>[19,20]</sup>

Compared with organic–inorganic halide perovskites, all-inorganic halide perovskites, such as cesium lead bromide (CsPbBr<sub>3</sub>), exhibit not only higher thermal and chemical stability, but also higher PLQY.<sup>[21–25]</sup> However, the EL efficiency of the CsPbBr<sub>3</sub>-based PeLEDs has yet been inferior to the MAPbBr<sub>3</sub>-based

PeLEDs. The factors limiting their performance are presented mainly in two aspects; the morphology of the perovskite films, and the interfaces between the perovskite emission layers and the charge-injection or transport layers. For a high-efficiency PeLED, the perovskite emission layer must have high quality morphology with high coverage and low defect density.<sup>[26]</sup> To passivate defects, reduce ion migration, and fabricate high-efficiency all-inorganic PeLEDs, one of the recent effective strategies is to introduce additives into the perovskite layers. Polymers, such as poly (ethylene oxide)<sup>[27,28]</sup> and polyethylene glycol,<sup>[29]</sup> have been employed into the perovskite precursors to passivate defects and suppress ion migration at grain boundaries. Another passivating agent is amine-based small molecules or polymers,<sup>[30,31]</sup> which also can improve the PLQYs and PL lifetimes of the perovskite films. Although the above passivating agents have the same feature of Lewis base and could produce similar effects on PL and EL improvement, the morphology of these perovskite films are multifarious, which is deduced to be the key of the different EL performance, enhanced with the different additives. However, how to choose the additives to control the perovskite polycrystalline morphology and suppress the defects at grain boundaries is still a big challenge in PeLEDs.

In addition to the control of the perovskite morphology to improve EL efficiency, the interface optimization is also vital to the device EL performance, because large

Dr. X. Liu, Dr. X. Guo, Dr. Y. Lv, Dr. Y. Hu, Dr. Y. Fan, Dr. J. Lin, Prof. X. Liu, Prof. X. Liu  
State Key Laboratory of Luminescence and Applications  
Changchun Institute of Optics  
Fine Mechanics and Physics  
Chinese Academy of Sciences  
Changchun 130033, P. R. China  
E-mail: guoxy@ciomp.ac.cn; liuxy@ciomp.ac.cn

Dr. X. Liu  
University of Chinese Academy of Sciences  
Beijing 100049, P. R. China

 The ORCID identification number(s) for the author(s) of this article can be found under <https://doi.org/10.1002/adom.201801245>.

DOI: 10.1002/adom.201801245

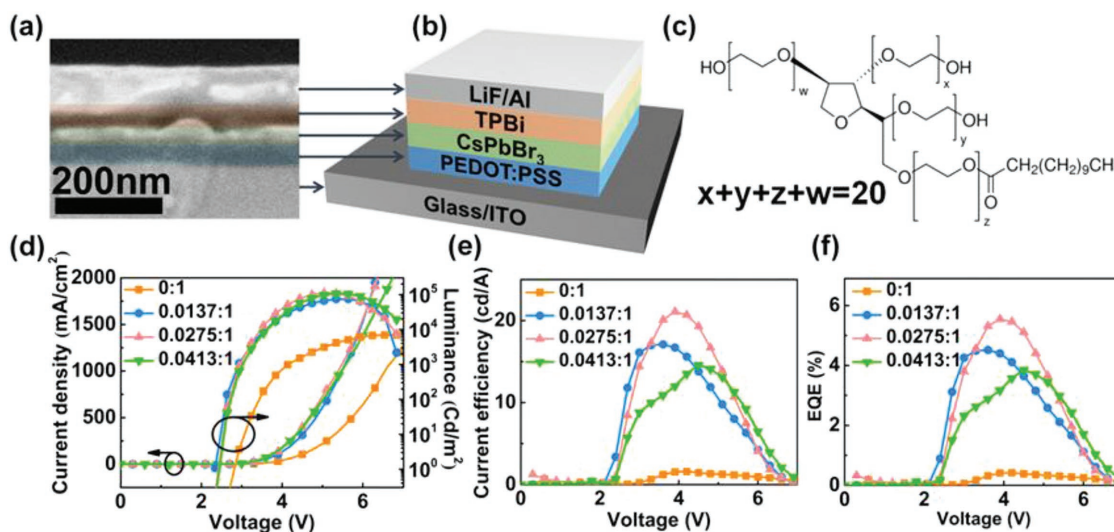


**Figure 1.** a) Cross-sectional SEM image and b) schematic representation of CsPbBr<sub>3</sub> PeLED. c) Molecule structure of Tween 20. d) *J*-*V* and *L*-*V*, e) *CE*-*V*, and f) *EQE*-*V* curves of PeLEDs with different Tween 20:CsPbBr<sub>3</sub> weight ratios.

energy barriers between the perovskite emission layers and the charge-injection or transport layers can hinder the charge injection, and charge unbalance in the perovskite films can reduce the radiative recombination. Several methods have been reported to modify the interface between the perovskite layers and the adjacent charge transport layer in the organic-inorganic-based PeLEDs,<sup>[8,32–35]</sup> such as employing ion-blocking layers between the perovskite layers and the hole transport layers to block the migration ions and passivate defects at the interfaces,<sup>[33,35]</sup> and adding polymers into the hole transport layer of poly(ethylenedioxythiophene):polystyrenesulfonate (PEDOT:PSS) to improve the hole injection.<sup>[8,32,34]</sup> However, the effect of the interface optimization has seldom been investigated in the all-inorganic CsPbBr<sub>3</sub> PeLEDs. Therefore, the optimization in both of the perovskite film and its adjacent interface layer is crucial to achieve high-efficiency all-inorganic PeLEDs.

In this work, a new passivating agent polyoxyethylene (20) sorbitan monolaurate (Tween 20) was introduced into the CsPbBr<sub>3</sub> film during fabrication of the all-inorganic PeLEDs. The Tween 20 also has a morphology-induced role during the formation of CsPbBr<sub>3</sub> film. Small grains arrange with each other along the plane direction and form large grains with reduced grain boundaries, which decrease the nonradiative recombination at the grain boundaries effectively, resulting in an enhanced PLQY (27%) and a prolonged exciton decay lifetime. The PeLED with Tween 20 passivated CsPbBr<sub>3</sub> film as the emission layer performs a highest brightness of 111 000 cd m<sup>-2</sup>, a peak CE of 21.1 cd A<sup>-1</sup>, and a maximum EQE of 5.55%. Meanwhile, the lifetime of the optimized PeLED has also been improved significantly in comparison with the PeLED based on neat CsPbBr<sub>3</sub> film. The device performance has been further improved by doping PEDOT:PSS with an anionic surfactant of sodium dodecyl benzene sulfonate (SDBS). An optimized PeLED with a highest brightness of 179 000 cd m<sup>-2</sup>, a peak CE of 28.0 cd A<sup>-1</sup>, and a maximum EQE of 7.39% was finally obtained. This work will provide new

thoughts and new methods for research and development of all-inorganic PeLEDs.

A conventional device structure of ITO/PEDOT:PSS/CsPbBr<sub>3</sub>/TPBi/LiF/Al has been employed in our work, the cross-sectional SEM image and schematic representation of CsPbBr<sub>3</sub>-based PeLEDs is shown in Figure 1a,b, and the molecule structure of the additive Tween 20 is shown in Figure 1c. PeLEDs with different Tween 20: CsPbBr<sub>3</sub> weight ratios as the emission layers have been fabricated, and Figure 1d–f shows the current density–voltage (*J*-*V*), luminance–voltage (*L*-*V*), *CE*-voltage (*CE*-*V*), as well as *EQE*-voltage (*EQE*-*V*) curves for these PeLEDs, and the detailed device parameters are summarized in Table 1. For the PeLED based on neat CsPbBr<sub>3</sub> film, it shows poor EL characteristics with a high turn-on voltage (*V*<sub>on</sub>) of 2.88 V, a maximum luminance of 6930 cd m<sup>-2</sup>, a maximum *CE* of 1.59 cd A<sup>-1</sup>, and a maximum *EQE* of 0.42%. As a small amount of Tween 20 was added into the perovskite precursor solution, the PeLEDs performance has been promoted significantly, and an optimized PeLED was obtained at the Tween 20:CsPbBr<sub>3</sub> weight ratio of 0.0275:1, exhibiting a *V*<sub>on</sub> of 2.48 V, a maximum luminance of 111 000 cd m<sup>-2</sup>, a peak *CE* of 21.1 cd A<sup>-1</sup>, and a peak *EQE* of 5.55%. The enhanced EL performance is considered to be the result from the defects passivated and ion migration suppressed at the grain boundaries. The EL spectrum of the PeLED displays a peak centered at 521 nm with a full width at half maximum (FWHM) of 17 nm and exhibits no obvious peak drift as the increased bias from

**Table 1.** Device parameters of PeLEDs.

Weight ratio (Tween 20:CsPbBr <sub>3</sub> )	<i>V</i> <sub>T</sub> [V]	<i>L</i> <sub>max</sub> [cd m <sup>-2</sup> ]	<i>CE</i> <sub>max</sub> [cd A <sup>-1</sup> ]	<i>EQE</i> <sub>max</sub> [%]
0:1	2.88	6930	1.59	0.42
0.0137:1	2.40	75 000	17.1	4.51
0.0275:1	2.48	111 000	21.1	5.55
0.0413:1	2.51	108 000	14.6	3.85

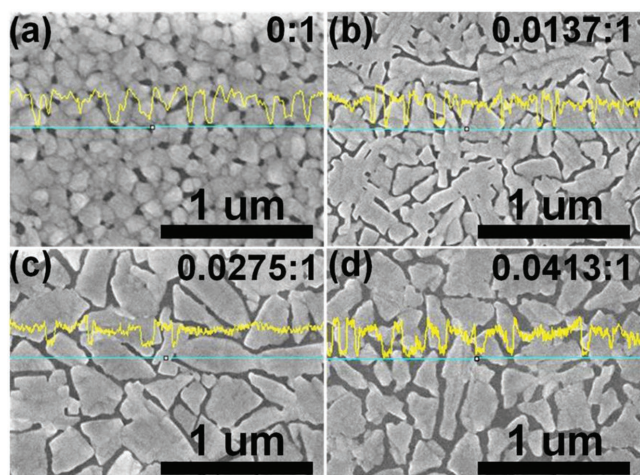


**Figure 2.** SEM images of perovskite films with various weight ratios (Tween 20:CsPbBr<sub>3</sub>): a) 0:1, b) 0.0137:1, c) 0.0275:1, and d) 0.0413:1. The line profiles are shown in the inset of each images. The film thicknesses are 33, 32, 29, and 25 nm, respectively.

4 to 6.5 V with a step of 0.5 V, performing pure green light emission with the Commission Internationale de l'Éclairage (CIE) color coordinate at (0.12, 0.79) (Figure S1, Supporting Information).

In order to explore the reason for the improved device properties and the effect of Tween 20 on CsPbBr<sub>3</sub> films, a series of measurements have been carried out. **Figure 2** shows the scanning electron microscope (SEM) images of CsPbBr<sub>3</sub> films with various weight ratios of Tween 20:CsPbBr<sub>3</sub>. For the pure CsPbBr<sub>3</sub> film (Figure 2a), it is mainly composed of small crystals with the grain size of about 100–200 nm, and together with a coverage of 82%. When a small amount of Tween 20 was introduced into the CsPbBr<sub>3</sub> films, some perovskite grains became interconnecting and thereby forming irregular large grains (Figure 2b). As the Tween 20:CsPbBr<sub>3</sub> ratio increased to 0.0275:1, the grains further arranged with each other along the plane direction, which can be seen clearly from the line profile with little fluctuation across the gathered grains. The well-arranged grains were enlarged to over 500 nm without coverage decreasing. Compared with the pure CsPbBr<sub>3</sub> film, the grain boundaries and traps would be sharply reduced due to the tightly arranged grains in the Tween 20:CsPbBr<sub>3</sub> films. Therefore, enhanced EL performance has been seen in the PeLED with Tween 20 doping in the emission layer (Figure 1d–f). However, as the Tween 20:CsPbBr<sub>3</sub> weight ratio was further increased to 0.0413:1, the grains become scattered again and the film coverage was decreased to 74%, which may result in increased grain gaps and boundaries, thus large leakage currents and degraded device performance.

To reveal the impact of introduced Tween 20 on the luminescent properties of CsPbBr<sub>3</sub> films, PL properties including steady-state and transient-state PL spectra, Raman PL mapping, and fluorescent PL images have been measured, which are shown in **Figure 3**. As shown in Figure 3a, the neat CsPbBr<sub>3</sub> film performs weaker green emission at 515 nm with a FWHM of 21 nm and a PLQY of 1%, while the Tween 20:CsPbBr<sub>3</sub> film exhibits strong PL intensity at 522 nm with

a FWHM of 17 nm and a PLQY of 27%. The dramatically increased PL emission indicates the reduction of nonradiative defects in the Tween 20:CsPbBr<sub>3</sub> film. In contrast to the neat CsPbBr<sub>3</sub> film, a small PL red-shift has been observed when the Tween 20 was added into the CsPbBr<sub>3</sub> film, which has also been seen in the absorption spectra (Figure S2a, Supporting Information). This phenomenon is consistent with the previous reports, which may be attributed to lattice strain, chemical composition variations, or assorted changes at the grain boundaries.<sup>[28,36,37]</sup> According to the X-ray diffraction (XRD) patterns (Figure S3, Supporting Information), similar spectra have been observed, indicating no obvious change for the perovskite crystal structure after introducing Tween 20, which excludes the impact by lattice strain. The X-ray photoelectron spectroscopy (XPS) spectra of the CsPbBr<sub>3</sub> films before and after doping Tween 20 have been shown in Figure S4 in the Supporting Information. It is found that the intensity of O peak has been increased after introducing Tween 20, and the high-resolution O 1s spectrum shows the existence of C–O–C at 532.48 eV and C=O at 531.12 eV, which confirms the existence of Tween 20 in the doped CsPbBr<sub>3</sub> film (Figure S4a,b, Supporting Information). Interestingly, the binding energies (BE) of Cs 3d, Pb 4f, and Br 3d all display a slight shift to the low BE after Tween 20 employing (Figure S4c–e, Supporting Information), which has been observed in the organic–inorganic halide perovskites.<sup>[38,39]</sup> The valence band maximum shows a consistent shift from 5.65 to 5.55 eV (Figure S4f, Supporting Information), indicating the PL red-shift probably originates from the change of the grain boundaries, but not chemical composition variations. The further component analysis of the perovskite films performed by Fourier transform infrared (FTIR) spectroscopy confirms the interaction between Tween 20 and Pb<sup>2+</sup> (Figure S5, Supporting Information), in which the stretching vibration frequency of C–O–C in Tween 20 has been shifted from 951 to 932 and 935 cm<sup>-1</sup> in Tween 20:PbBr<sub>2</sub> and Tween 20:CsPbBr<sub>3</sub> samples, respectively.<sup>[29,40,41]</sup> According to the above discussion, we deduce that the Lewis base Tween 20 combined with the Lewis acid Pb<sup>2+</sup> at the grain boundaries, inducing the formation of the well-arranged grains along the plane direction, and highly passivating the defects at the grain boundaries. The average lifetimes ( $\tau_{\text{avg}}$ ) for neat CsPbBr<sub>3</sub> and Tween 20:CsPbBr<sub>3</sub> films have been extracted from the PL decay curves (Table S1, Supporting Information), an enhanced PL lifetime of 48.68 ns is obtained, comparing with the neat CsPbBr<sub>3</sub> film of 11.94 ns (Figure 3b) due to the highly suppressed nonradiative decay of the Tween 20:CsPbBr<sub>3</sub> film.

Moreover, PL mapping and fluorescent images of the neat CsPbBr<sub>3</sub> and Tween 20:CsPbBr<sub>3</sub> films have been displayed in Figure 3c–f, respectively, which show the visual evidence of the effect of Tween 20. A colorful image is seen in Figure 3c, which illustrates the drastic fluctuation of the PL intensities. And the obvious changes of the brightness in Figure 3e also prove the inhomogeneous emission in the neat CsPbBr<sub>3</sub> film. Compared with the neat CsPbBr<sub>3</sub> film (Figure 3c,e), the PL intensity distribution of the Tween 20–CsPbBr<sub>3</sub> film is seen more uniform and stronger (Figure 3d,f), indicating the reduced defects and ion migration at the grain boundaries, thus enhancing the PeLED performance. The decreased nonradiative decay rate

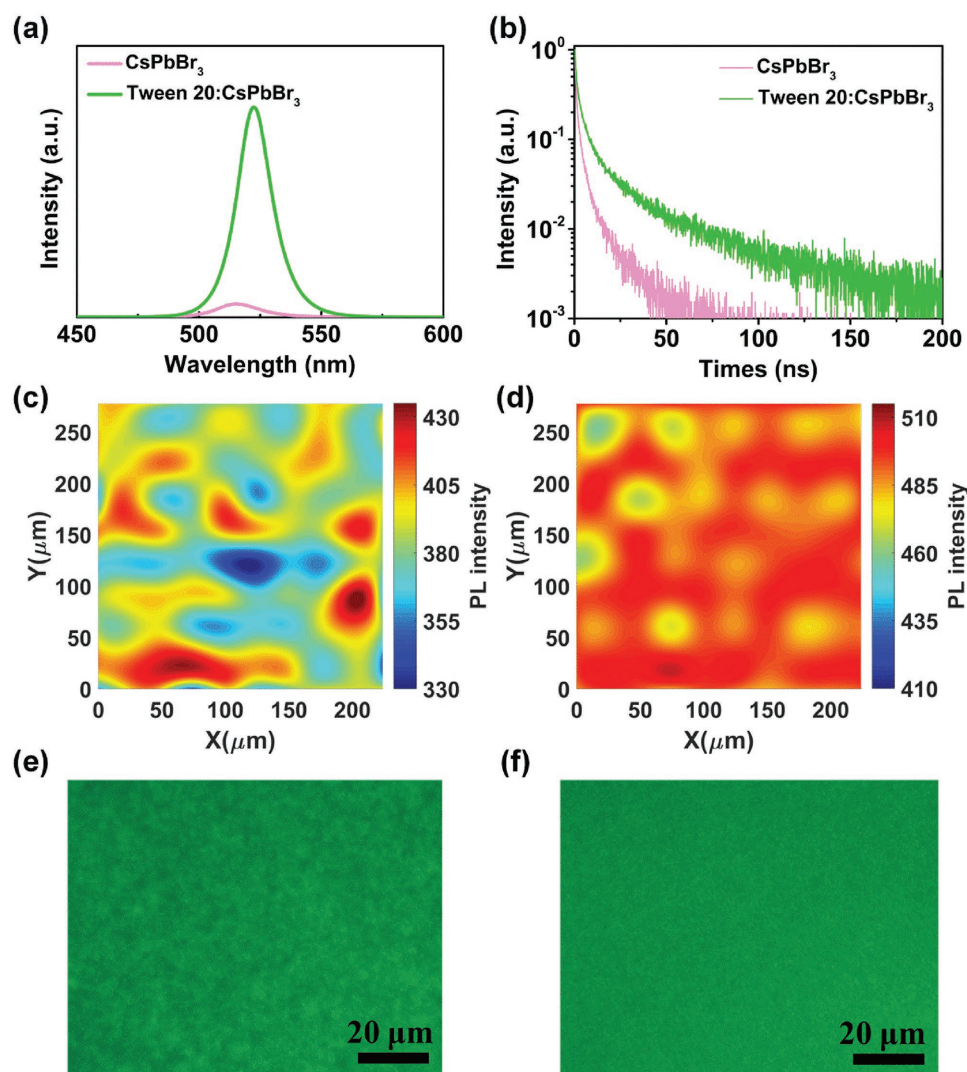


**Figure 3.** a) PL and b) time-resolved PL (TRPL) spectra of neat CsPbBr<sub>3</sub> and Tween 20:CsPbBr<sub>3</sub> (0.0275:1) thin films. c,d) PL mapping and e,f) fluorescent images of neat CsPbBr<sub>3</sub> and Tween 20:CsPbBr<sub>3</sub> (0.0275:1) thin films.

from  $8.3 \times 10^7$  to  $1.5 \times 10^7$  s<sup>-1</sup> also can verify the decreased defects, which can be extracted as follows:

$$\text{PLQY} = \frac{k_r}{(k_r + k_{nr})} \quad (1)$$

$$\tau_{\text{avg}} = \frac{1}{(k_r + k_{nr})} \quad (2)$$

where  $k_r$  and  $k_{nr}$  represent the radiative and nonradiative decay rates, respectively.

In previous works of PeLEDs, it was found that the electron transporting ability was higher than that of the hole, resulting in charge unbalance during recombination luminescence.<sup>[27]</sup> In order to further optimize the PeLED performance, an anionic surfactant SDBS was chosen to add into the PEDOT:PSS layer for improving the conductivity of PEDOT:PSS and enhancing the hole injection. **Figure 4** shows the EL performance of the

PeLEDs fabricated on PEDOT:PSS substrates with various concentrations of SDBS, and the EL parameters are listed in **Table 2**. As the SDBS concentration increases, the device characteristics including CE, EQE, and maximum luminance have been improved steadily, and achieves the best performance with a SDBS concentration of 3.64 mg mL<sup>-1</sup>. The optimized device shows a highest luminance of 179 000 cd m<sup>-2</sup>, a peak CE of 28.0 cd A<sup>-1</sup>, and a maximum EQE of 7.39%, which is among the highest values of the reported PeLEDs based on CsPbBr<sub>3</sub> films (Table S2, Supporting Information). Several measurements have been carried out to reveal the effect of the modified PEDOT:PSS on the devices. Due to the slight SDBS amount, the morphologies of the modified PEDOT:PSS and the perovskites deposited above along with the work function of the modified PEDOT:PSS layer are almost consistent with the untreated PEDOT:PSS layer (Figures S6–S8, Supporting Information). But the conductivity of the modified PEDOT:PSS has been increased by a factor of 55 (from 0.002

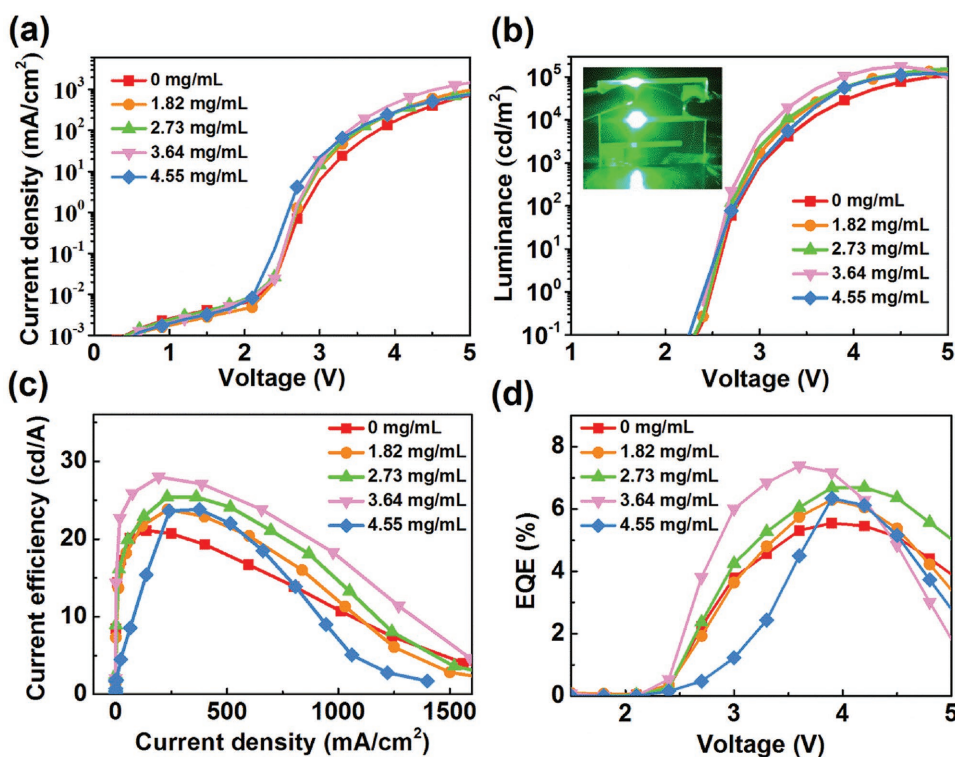


**Figure 4.** a)  $J$ - $V$  curves. b)  $L$ - $V$  curves. c)  $CE$ - $J$  curves. d)  $EQE$ - $V$  curves of the PeLEDs with different SDBS concentrations. The photo of the working device is shown in the inset of Figure 4b.

to  $0.11 \text{ S cm}^{-1}$ ), which has also been observed in the previous report.<sup>[42–44]</sup> The conductivity enhancement mechanism of the modified PEDOT:PSS can be attributed to the reduction of the distortion of the PEDOT chain after the SDBS treatment,<sup>[42]</sup> and the decreased root mean square (RMS) roughness from 2.21 for the neat PEDOT:PSS film to 1.90 nm for the modified PEDOT:PSS film maybe an indirect evidence (Figure S7, Supporting Information).

As a result, the hole can inject more efficiently, and achieve a more ideal charge balance, which has been confirmed by the hole-only devices shown in Figure 5a. The structures of hole-only devices are ITO/PEDOT:PSS/neat CsPbBr<sub>3</sub>/MoO<sub>3</sub>/Al (device A), ITO/PEDOT:PSS/Tween 20:CsPbBr<sub>3</sub>/MoO<sub>3</sub>/Al (device B), and ITO/SDBS-PEDOT:PSS/Tween 20:CsPbBr<sub>3</sub>/MoO<sub>3</sub>/Al (device C), respectively. Device A shows the lowest hole current density, while the hole current density of device B increases substantially due to the highly passivated defects and traps at the grain boundaries, verified by the reduced defect

density in the Tween 20:CsPbBr<sub>3</sub> film (Figure S9, Supporting Information). The hole current density of device C further improves with the modified PEDOT:PSS film. The enhanced hole current density indicates that the charge injection and transport are more balanced, thus raising the radiative recombination efficiency and boosting the PeLED performance.

The stabilities of these devices have been surveyed by the time-dependent EL measured under a constant applied current in air (50% relative humidity) without encapsulation, which has been shown in Figure 5b. Neat CsPbBr<sub>3</sub> film-based PeLED shows a severe degradation, it took only several minutes for the lifespan to decline by half, which are mainly caused by the existing defects and traps at the grain boundaries. Compared with the controlled PeLED, the device based on Tween 20:CsPbBr<sub>3</sub> film shows a significantly enhanced stability with a lifetime of about 4.5 h under the same condition, which is contributed to the passivated boundaries and reduced defect densities of Tween 20:CsPbBr<sub>3</sub>. In the meanwhile, the lifetime of PeLED is further prolonged to nearly 6 h with the SDBS doped PEDOT:PSS film, indicating the balanced charge carriers are beneficial to improve the stability of the PeLEDs.

Although the EL performance has improved significantly by introducing Tween 20 into the CsPbBr<sub>3</sub> film, the thin emission layer resulted uncontinuous Tween 20:CsPbBr<sub>3</sub> film would restrict the device performance in some degree. We believe the EL performance would be further promoted if a more condensed Tween 20:CsPbBr<sub>3</sub> film formed. Efforts are still needed to improve the quality of the all inorganic perovskite film and further study the related physical mechanism.

**Table 2.** The device parameters of improved PeLEDs.

SDBS [mg mL <sup>-1</sup> ]	$V_T$ [V]	$L_{max}$ [cd m <sup>-2</sup> ]	$CE_{max}$ [cd A <sup>-1</sup> ]	$EQE_{max}$ [%]
0	2.48	111 000	21.1	5.55
1.82	2.47	134 000	22.9	6.30
2.73	2.47	157 000	25.4	6.70
3.64	2.43	179 000	28.0	7.39
4.55	2.41	137 000	24.0	6.34

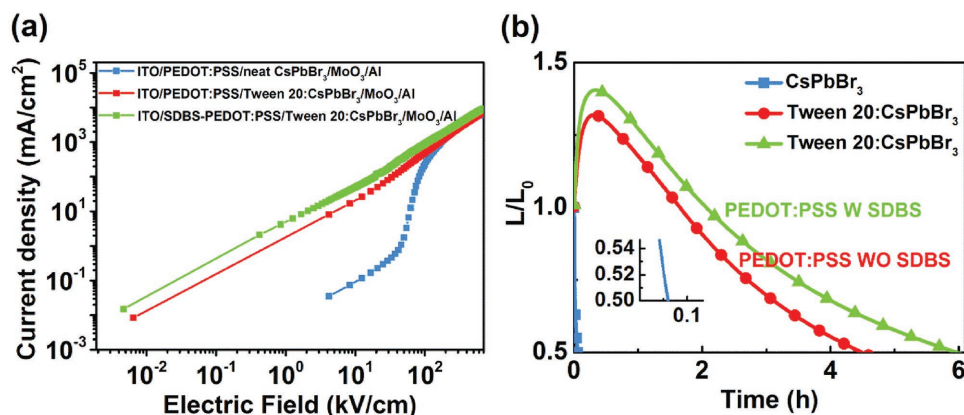


**Figure 5.** a) The  $J$ - $F$  curves of hole-only devices (ITO/PEDOT:PSS/neat CsPbBr<sub>3</sub>/MoO<sub>3</sub>/Al, ITO/PEDOT:PSS/Tween 20:CsPbBr<sub>3</sub>/MoO<sub>3</sub>/Al, and ITO/SDBS-PEDOT:PSS/Tween 20:CsPbBr<sub>3</sub>/MoO<sub>3</sub>/Al). b) Operational lifetime of PeLEDs based on neat CsPbBr<sub>3</sub>, Tween 20:CsPbBr<sub>3</sub> films (PEDOT:PSS without SDBS), Tween 20:CsPbBr<sub>3</sub> films (PEDOT:PSS with SDBS) ( $L_0 = 100$  cd m<sup>-2</sup>).

In summary, the performance and stability of all-inorganic PeLEDs have been promoted by morphology and interface engineering. A nonionic surfactant Tween 20 was introduced into the all-inorganic CsPbBr<sub>3</sub> emission layer, significantly enhancing the PLQY by passivating the defects and traps at the grain boundaries. The optimal device shows a highest brightness of 111 000 cd m<sup>-2</sup>, a peak CE of 21.1 cd A<sup>-1</sup>, a maximum EQE of 5.55%, together with an operational lifetime of 4.5 h under ambient condition. The EL performance of the all-inorganic PeLED has been further improved by using a SDBS modified PEDOT:PSS as the hole injection layer. More balanced charge injection and transport enable more efficient radiative recombination, realizing a high efficient PeLED with an ultra-high brightness of 179 000 cd m<sup>-2</sup>, together with a peak CE of 28.0 cd A<sup>-1</sup>, a maximum EQE of 7.39%, and a prolonged lifetime of 6 h. This work will be beneficial to the promotion of all-inorganic PeLEDs.

## Experimental Section

**Materials:** CsBr (99.9%), PbBr<sub>2</sub> (99.9%), PEDOT:PSS, and TPBi were purchased from Xi'an Polymer Light Technology Corp. All the above chemicals were used directly without further purification.

**Perovskite Film Fabrication and Characterization:** CsBr and PbBr<sub>2</sub> were dissolved in anhydrous DMSO with a concentration of 145 mg mL<sup>-1</sup>, the molar ratio between CsBr and PbBr<sub>2</sub> was 1.86:1. Tween 20 was dissolved in anhydrous DMSO with a concentration of 20 mg mL<sup>-1</sup>. These two solutions were blended at various Tween 20:CsPbBr<sub>3</sub> weight ratios before fabricating perovskite films, 120  $\mu$ L mixed solution was dropped on the center of prepared substrates and spin-coated at a speed of 5000 rpm for 1 min, and then dried at 70 °C for 10 min. The film coverage was calculated by a software of Image J. The SEM images and the XRD patterns of perovskite films were measured, respectively, by a Hitachi S4800 microscope and Rigaku D/Max-2500 diffractometer (Cu K $\alpha$ ,  $\lambda = 1.54$  Å). The absorption spectra were measured by Shimadzu UV-3101 PC spectrophotometer. The PL spectra were acquired by using Hitachi fluorescence spectrometer F-7000. The time-resolved PL (TRPL) spectra decay measurements were conducted on an Edinburgh FLS920 spectrometer at an excitation wavelength of 375 nm. PL mapping was measured by using the 325 nm line of a He-Cd laser as excitation source in a LabRAM-UV Jobin Yvon spectrometer. FTIR spectra were conducted by using a PerkinElmer FTIR spectrometer. The fluorescent

images were conducted by C2+ confocal microscope system (Nikon confocal instruments). The thicknesses were conducted by a surface profiler (XP-1, Ambios, USA). The sheet resistances were measured by using a four-probe method. Atomic force microscope images were measured on a Shimadzu SPM-9700 (Shimadzu Corp., Japan). Ultraviolet photoelectron spectroscopy and XPS studies were obtained using a Thermo ESCALAB 250 instrument with a helium discharge lamp at  $h\nu = 21.22$  eV and Al K $\alpha$  X-rays ( $h\nu = 1486.6$  eV), respectively. The C 1s peak at 284.5 eV was considered the standard for all charge shift corrections during the peak fitting process.

**Devices Fabrication and Characterization:** PeLEDs were constructed on ITO electrodes, which were cleaned with the mixed solutions of ethanol and ether for 20 min by sonication, and then treated by oxygen plasma for 15 min. Filtered PEDOT:PSS or SDBS modified PEDOT:PSS was spin-coated on the prepared ITO electrodes at 3500 rpm for 40 s, then baked at 140 °C for 15 min. Afterwards, the substrates were transferred to a N<sub>2</sub> filled glovebox for the perovskite film deposition. TPBi, LiF, and Al were deposited successively in a thermal evaporation chamber at a pressure of  $5.0 \times 10^{-5}$  Pa. The effective area of devices was 0.01 cm<sup>2</sup>. All measurements were performed in air without encapsulation. Current density-voltage-luminance ( $J$ - $V$ - $L$ ) characteristics of PeLEDs were measured using a Keithley 2400 source meter and a luminance meter (LS-110, Konica Minolta). EL spectra were recorded by an Avantes Avaspec 2048 spectrometer.

## Supporting Information

Supporting Information is available from the Wiley Online Library or from the author.

## Acknowledgements

This work was supported by the National Natural Science Foundation of China No. 61774154, 51503196, 61704170, and 61775211, the Jilin Province Science and Technology Research Project No. 20180201029GX, 20170101039JC, 20160520176JH, and 20160520092JH, and project supported by Dawn Talent Training Program of CIOMP.

## Conflict of Interest

The authors declare no conflict of interest.

## Keywords

CsPbBr<sub>3</sub>, device stability, interface engineering, perovskite light-emitting diodes, surface passivation

Received: September 12, 2018

Revised: October 16, 2018

Published online: October 29, 2018

- [1] W. S. Yang, J. H. Noh, N. J. Jeon, Y. C. Kim, S. Ryu, J. Seo, S. I. Seok, *Science* **2015**, *348*, 1234.
- [2] D. P. McMeekin, G. Sadoughi, W. Rehman, G. E. Eperon, M. Saliba, M. T. Hoerantner, A. Haghighirad, N. Sakai, L. Korte, B. Rech, M. B. Johnston, L. M. Herz, H. J. Snaith, *Science* **2016**, *351*, 151.
- [3] Y.-C. Zhao, W.-K. Zhou, X. Zhou, K.-H. Liu, D.-P. Yu, Q. Zhao, *Light Sci. Appl.* **2016**, *6*, e16243.
- [4] W. S. Yang, B.-W. Park, E. H. Jung, N. J. Jeon, Y. C. Kim, D. U. Lee, S. S. Shin, J. Seo, E. K. Kim, J. H. Noh, S. I. Seok, *Science* **2017**, *356*, 1376.
- [5] H.-H. Fang, F. Wang, S. Adjokatse, N. Zhao, J. Even, M. A. Loi, *Light Sci. Appl.* **2016**, *5*, e16056.
- [6] Z.-K. Tan, R. S. Moghaddam, M. L. Lai, P. Docampo, R. Higler, F. Deschler, M. Price, A. Sadhanala, L. M. Pazos, D. Credgington, F. Hanusch, T. Bein, H. J. Snaith, R. H. Friend, *Nat. Nanotechnol.* **2014**, *9*, 687.
- [7] G. Li, Z.-K. Tan, D. Di, M. L. Lai, L. Jiang, J. H.-W. Lim, R. H. Friend, N. C. Greenham, *Nano Lett.* **2015**, *15*, 2640.
- [8] H. Cho, S.-H. Jeong, M.-H. Park, Y.-H. Kim, C. Wolf, C.-L. Lee, J. H. Heo, A. Sadhanala, N. Myoung, S. Yoo, S. H. Im, R. H. Friend, T.-W. Lee, *Science* **2015**, *350*, 1222.
- [9] G. Xing, N. Mathews, S. S. Lim, N. Yantara, X. Liu, D. Sabba, M. Gratzel, S. Mhaisalkar, T. C. Sum, *Nat. Mater.* **2014**, *13*, 476.
- [10] H. Zhu, Y. Fu, F. Meng, X. Wu, Z. Gong, Q. Ding, M. V. Gustafsson, M. T. Trinh, S. Jin, X. Y. Zhu, *Nat. Mater.* **2015**, *14*, 636.
- [11] L. Gu, Z. Fan, *Light Sci. Appl.* **2017**, *6*, e17090.
- [12] C. Xie, P. You, Z. Liu, L. Li, F. Yan, *Light Sci. Appl.* **2017**, *6*, e17023.
- [13] S. Tong, J. Sun, C. Wang, Y. Huang, C. Zhang, J. Shen, H. Xie, D. Niu, S. Xiao, Y. Yuan, J. He, J. Yang, Y. Gao, *Adv. Electron. Mater.* **2017**, *3*, 1700058.
- [14] X. Li, Y. Wu, S. Zhang, B. Cai, Y. Gu, J. Song, H. Zeng, *Adv. Funct. Mater.* **2016**, *26*, 2435.
- [15] N. K. Kumawat, A. Dey, A. Kumar, S. P. Gopinathan, K. L. Narasimhan, D. Kabra, *ACS Appl. Mater. Interfaces* **2015**, *7*, 13119.
- [16] F. Deschler, M. Price, S. Pathak, L. E. Klintberg, D.-D. Jarausch, R. Higler, S. Huettner, T. Leijtens, S. D. Stranks, H. J. Snaith, M. Atatuere, R. T. Phillips, R. H. Friend, *J. Phys. Chem. Lett.* **2014**, *5*, 1421.
- [17] F. Zhang, H. Zhong, C. Chen, X.-g. Wu, X. Hu, H. Huang, J. Han, B. Zou, Y. Dong, *ACS Nano* **2015**, *9*, 4533.
- [18] X. Yang, X. Zhang, J. Deng, Z. Chu, Q. Jiang, J. Meng, P. Wang, L. Zhang, Z. Yin, J. You, *Nat. Commun.* **2018**, *9*, 570.
- [19] J. C. Yu, D. W. Kim, B. Kim da, E. D. Jung, J. H. Park, A. Y. Lee, B. R. Lee, D. Di Nuzzo, R. H. Friend, M. H. Song, *Adv. Mater.* **2016**, *28*, 6906.
- [20] C. Sun, Y. Zhang, C. Ruan, C. Yin, X. Wang, Y. Wang, W. W. Yu, *Adv. Mater.* **2016**, *28*, 10088.
- [21] J. Song, J. Li, X. Li, L. Xu, Y. Dong, H. Zeng, *Adv. Mater.* **2015**, *27*, 7162.
- [22] L. Protesescu, S. Yakunin, M. I. Bodnarchuk, F. Krieg, R. Caputo, C. H. Hendon, R. X. Yang, A. Walsh, M. V. Kovalenko, *Nano Lett.* **2015**, *15*, 3692.
- [23] M. Kulbak, D. Cahen, G. Hodes, *J. Phys. Chem. Lett.* **2015**, *6*, 2452.
- [24] N. Yantara, S. Bhaumik, F. Yan, D. Sabba, H. A. Dewi, N. Mathews, P. P. Boix, H. V. Demir, S. Mhaisalkar, *J. Phys. Chem. Lett.* **2015**, *6*, 4360.
- [25] X. Zhang, B. Xu, J. Zhang, Y. Gao, Y. Zheng, K. Wang, X. W. Sun, *Adv. Funct. Mater.* **2016**, *26*, 4595.
- [26] H. Cho, C. Wolf, J. S. Kim, H. J. Yun, J. S. Bae, H. Kim, J.-M. Heo, S. Ahn, T.-W. Lee, *Adv. Mater.* **2017**, *29*, 1700579.
- [27] Y. Ling, Y. Tian, X. Wang, J. C. Wang, J. M. Knox, F. Perez-Orive, Y. Du, L. Tan, K. Hanson, B. Ma, H. Gao, *Adv. Mater.* **2016**, *28*, 8983.
- [28] C. Wu, Y. Zou, T. Wu, M. Ban, V. Pecunia, Y. Han, Q. Liu, T. Song, S. Duhm, B. Sun, *Adv. Funct. Mater.* **2017**, *27*, 1700338.
- [29] L. Song, X. Guo, Y. Hu, Y. Lv, J. Lin, Z. Liu, Y. Fan, X. Liu, *J. Phys. Chem. Lett.* **2017**, *8*, 4148.
- [30] Z. Xiao, R. A. Kerner, L. Zhao, N. L. Tran, K. M. Lee, T.-W. Koh, G. D. Scholes, B. P. Rand, *Nat. Photonics* **2017**, *11*, 108.
- [31] S. Lee, J. H. Park, B. R. Lee, E. D. Jung, J. C. Yu, D. Di Nuzzo, R. H. Friend, M. H. Song, *J. Phys. Chem. Lett.* **2017**, *8*, 1784.
- [32] X.-F. Peng, X.-Y. Wu, X.-X. Ji, J. Ren, Q. Wang, G.-Q. Li, X.-H. Yang, *J. Phys. Chem. Lett.* **2017**, *8*, 4691.
- [33] S. A. Veldhuis, P. P. Boix, N. Yantara, M. Li, T. C. Sum, N. Mathews, S. G. Mhaisalkar, *Adv. Mater.* **2016**, *28*, 6804.
- [34] Y.-H. Kim, H. Cho, J. H. Heo, T.-S. Kim, N. Myoung, C.-L. Lee, S. H. Im, T.-W. Lee, *Adv. Mater.* **2015**, *27*, 1248.
- [35] H. Cho, Y.-H. Kim, C. Wolf, H.-D. Lee, T.-W. Lee, *Adv. Mater.* **2018**, *30*, 1704587.
- [36] D. W. deQuilettes, S. Koch, S. Burke, R. K. Paranjhi, A. J. Shropshire, M. E. Ziffer, D. S. Ginger, *ACS Energy Lett.* **2016**, *1*, 438.
- [37] W. Nie, H. Tsai, R. Asadpour, J.-C. Blancon, A. J. Neukirch, G. Gupta, J. J. Crochet, M. Chhowalla, S. Tretiak, M. A. Alam, H.-L. Wang, A. D. Mohite, *Science* **2015**, *347*, 522.
- [38] Z. Su, Y. Chen, X. Li, S. Wang, Y. Xiao, *J. Mater. Sci.: Mater. Electron.* **2017**, *28*, 11053.
- [39] F.-S. Zu, P. Amsalem, I. Salzmann, R.-B. Wang, M. Ralaiarisoa, S. Kowarik, S. Duhm, N. Koch, *Adv. Opt. Mater.* **2017**, *5*, 1700139.
- [40] Y. L. Su, J. Wang, H. Z. Liu, *J. Colloid Interface Sci.* **2002**, *251*, 417.
- [41] X. Zhang, H. Yin, X. Cheng, H. Hu, Q. Yu, A. Wang, *Mater. Res. Bull.* **2006**, *41*, 2041.
- [42] B. Fan, X. Mei, J. Ouyang, *Macromolecules* **2008**, *41*, 5971.
- [43] N. Kishi, Y. Kondo, H. Kunieda, S. Hibi, Y. Sawada, *J. Mater. Sci.: Mater. Electron.* **2018**, *29*, 4030.
- [44] N. Romyen, S. Thongyai, P. Praserttham, S. Wacharawichanant, *J. Electron. Mater.* **2017**, *46*, 6709.